Journal of Medicinal Chemistry Article

J. Med. Chem. **2010,** *53,* 3095–3105 **3095**
DOI: 10.1021/jm901718z

Pharmacophore Development and Application Toward the Identification of Novel, Small-Molecule Autotaxin Inhibitors

E. Jeffrey North,[†,‡] Angela L. Howard,[†,‡] Irene W. Wanjala,[†,‡] Truc Chi T. Pham,[†] Daniel L. Baker,*[,†] and Abby L. Parrill*[,†,‡]

[†]*Department of Chemistry and* [‡]*Computational Research on Materials Institute, The University of Memphis, Memphis, Tennessee 38152*

Received November 20, 2009

Autotaxin (ATX) is a secreted glycoprotein with lysophospholipase D (LPLD) activity that generates the bioactive lipid lysophosphatidic acid (LPA) from lysophosphatidylcholine (LPC). Both ATX and LPA have been linked to the promotion and progression of cancer as well as cardiovascular disease and obesity. Despite the fact that ATX inhibitors have the potential to be useful chemotherapeutics for multiple indications, few examples of potent ATX inhibitors are described in the current literature. Here we describe the development of pharmacophore models for the inhibition of ATX by nonlipids and apply these tools to the discovery of additional ATX inhibitors using the NCI open chemical repository database. From this database of >250000 compounds, 168 candidate inhibitors were identified. Of these candidates, 106 were available for testing and 33 were identified as active (those that inhibited ATX activity by ≥50% at a single 10 μM concentration), a 31% hit rate. Five of these compounds had $IC_{50} < 1.5$ μM and the most potent compound possessed a K_i of 271 nM.

Introduction

Autotaxin (ATX[a]) is a 125 kDa glycoprotein, originally identified as an autocrine motility factor derived from media conditioned by the A2058 melanoma cell line.[1] In 2002, the biological effects of ATX were linked to its ability to hydrolyze lysophosphotidylcholine (LPC) to form the bioactive lipid lysophosphatidic acid (LPA).[2,3] LPA elicits a variety of biological responses including stimulation of cell proliferation, survival, motility, and wound healing through activation of specific G protein-coupled receptors (GPCR), LPA_{1-8}.[4−10] Significant literature exists linking ATX and LPA to the promotion and progression of various cancers.[11−17] In addition, it is becoming increasingly clear that ATX and LPA also play critical roles in normal development[18−20] and in additional human pathologies such as Alzheimer's disease,[21] rheumatoid arthritis,[22] obesity,[23] and neuropathic pain.[24] Blocking the effects of LPA has the potential to provide positive anticancer chemotherapeutic and other health benefits. This strategy can be achieved at the receptor level, with LPA antagonists and inverse agonists, or through ATX inhibition to prevent LPA production. In 2005, LPA and sphingosine 1-phosphate (S1P) were identified as negative feedback inhibitors of ATX,[25] which spurred efforts to synthesize and evaluate lipid-like product analogues for ATX inhibition.[25−35] However, these analogues must lack agonist activity at LPA and S1P GPCR to be useful therapeutic candidates. In addition, LPA and S1P analogues are likely to have poor oral bioavailability due to their hydrophobicity and are likely to be rapidly degraded by endogenous hydrolytic pathways. Collectively, lipid-based analogues possess low structural diversity and high numbers of rotatable bonds, which limits their utility as tools to be used in computational efforts to identify novel ATX inhibitors.

Only recently have nonlipid ATX inhibitors begun to emerge in the literature.[36−38] Figure 1 shows examples of three previously identified nonlipid ATX inhibitors. Multiple inhibitors such as H2L 7905958 (Figure 1) were previously identified from database screening efforts using a binary QSAR model.[37] ATX inhibitors such as damnacanthal (Figure 1) were originally identified as protein kinase inhibitors and therefore are not specific ATX inhibitors.[38] Additional novel, nonlipid ATX inhibitors are likely to provide important insight into the three-dimensional structure of the ATX active site, for which little data currently exists due to a lack of biophysical data such as X-ray diffraction or NMR characterization.

Here we describe the development of ligand-based pharmacophore models using previously published nonlipid ATX inhibitors.[37] These models were used to search the National Cancer Institute (NCI) open chemical repository database (http://dtp.cancer.gov) to identify novel, nonlipid ATX inhibitor leads. These inhibitors have been validated using two assays, one utilized the synthetic, FRET-based, ATX substrate FS-3, and a second used the endogenous ATX substrate LPC in a choline release assay. Filtering of the database using nine related pharmacophore models resulted in the identification of several potent ATX inhibitors. This strategy identified active ATX inhibitors (those providing ≥50% inhibition of ATX-mediated FS-3 hydrolysis at a single 10 μM dose) at an overall 31% hit rate. The most potent of these newly identified compounds were further characterized via the determination

*To whom correspondence should be addressed. Phone: (901) 678-2638 (A.L.P.); (901) 678-4178 (D.L.B.). Fax: (901) 678-3447. E-mail: aparrill@memphis.edu (A.L.P.); dlbaker@memphis.edu (D.L.B.).

[a] Abbreviations: ATX, autotaxin; NPP, nucleotide pyrophosphatase/phosphodiesterase; LPA, lysophosphatidic acid; LPC, lysophosphatidylcholine; GPCR, G protein-coupled receptor; S1P, sphingosine 1-phosphate; FRET, fluorescence resonance energy transfer; NCI, National Cancer Institute; BSA, bovine serum albumin; pNPPC, *para*-nitrophenylphosphocholine.

Published on Web 03/29/2010

of IC_{50} and K_i values for ATX inhibition and selectivity for related NPP isoforms.

Results

To develop a pharmacophore for ATX inhibition, the structures of eight previously identified nonlipid ATX inhibitors[37] (Figure 2) were built using the Molecular Operating Environment (MOE) software[39] and ionized as predicted at pH 7.4. These compounds were then flexibly aligned to one another to identify functional groups sharing common volumes. Six pharmacophore points were identified in at least five of the eight compounds, including one anionic group (point 1), two hydrogen bond acceptors/metal ligators (points 2 and 4), two aromatic groups (points 3 and 5), and one hydrogen bond donor (point 6) (Figures 2 and 3). To determine if this six-point model was overly restrictive

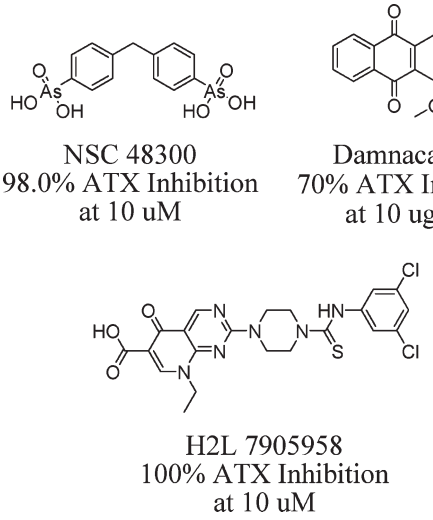

Figure 1. Representative previously identified nonlipid ATX inhibitors.[25−33,35]

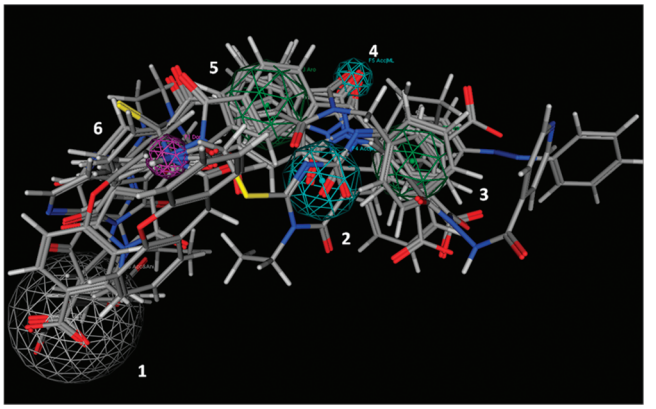

Figure 3. Flexible alignment of the eight previously identified ATX inhibitors with the pharmacophore points encompassing overlapping functional groups. Point 1, anionic group; points 2 and 4, H-bond acceptor/metal ligators; points 3 and 5, aromatic groups; point 6, H-bond donor.

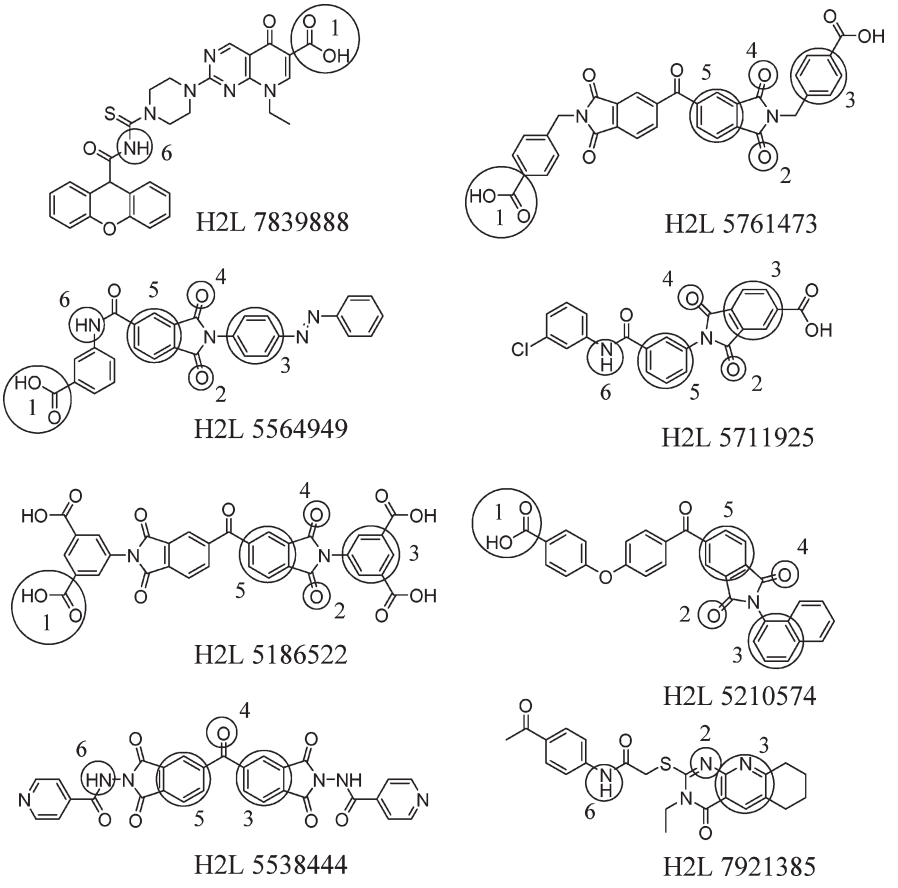

Figure 2. Previously published ATX inhibitors used to develop the flexible alignment from which subsequent pharmacophore models were derived.[37] The circled and numbered functional groups gave rise to the pharmacophore features (1, anionic group; 2 and 4, H-bond acceptor/metal ligators; 3 and 5, aromatic groups; 6, H-bond donor).

Table 1. Pharmacophore Point Distances and Ranges Used to Search the NCI Open Chemical Repository

pharmacophore 6 (points 1, 2, 3, 4, 5, and 6)		
points	distance (Å)	range searched (Å)
1−3	15.04	14−16
1−4	14.82	14−16
2−5	3.66	2−5
3−5	5.97	5−7
3−6	9.25	8−10.5
4−6	7.93	7−9

pharmacophore 5a (points 1, 3, 4, 5, and 6)		
points	distance (Å)	range searched (Å)
1−3	15.04	14−16
1−4	14.82	14−16
1−6	8.86	8−10
3−5	5.97	5−7
3−6	9.25	8−10.5
4−6	7.93	7−9

pharmacophore 5b (1, 2, 4, 5, and 6)		
points	distance (Å)	range searched (Å)
1−2	11.96	10−14
1−4	14.82	14−16
2−4	4.58	3.5−6.5
2−5	3.66	2−5
2−6	5.68	4−7
4−6	7.93	7−9

pharmacophore 5c (points 1, 2, 3, 5, and 6)		
points	distance (Å)	range searched (Å)
1−2	11.96	10−14
1−5	11.82	11−13
2−3	3.77	3−5
2−6	5.68	4−7
3−5	5.97	5−7
5−6	4.32	3−5

pharmacophore 5d (points 1, 2, 3, 4, and 6)		
points	distance (Å)	range searched (Å)
1−2	11.96	10−14
1−3	15.04	14−16
1−4	14.82	14−16
2−4	4.58	3.5−6.5
3−6	9.25	8−10.5
4−6	7.93	7−9

pharmacophore 4a (points 1, 2, 3, and 6)		
points	distance (Å)	range searched (Å)
1−2	11.96	10−14
1−3	15.04	14−16
1−6	8.86	8−10
2−3	3.77	3−5
2−6	5.68	4−7
3−6	9.25	8−10.5

pharmacophore 4b (points 1, 2, 5, and 6)		
points	distance (Å)	range searched (Å)
1−2	11.96	10−14
1−5	11.82	11−13
1−6	8.86	8−10
2−5	3.66	2−5
2−6	5.68	4−7
5−6	4.32	3−5

pharmacophore 4c (points 1, 3, 4, and 6)		
points	distance (Å)	range searched (Å)
1−3	15.04	14−16
1−4	14.82	14−16
1−6	8.86	8−10
3−4	3.97	3−5
3−6	9.25	8−10.5
4−6	7.93	7−9

pharmacophore 4d (points 1, 4, 5, and 6)		
points	distance (Å)	range searched (Å)
1−4	14.82	14−16
1−5	11.82	11−13
1−6	8.86	8−10
4−5	3.66	2.5−4.5
4−6	7.93	7−9
5−6	4.32	3−5

and to evaluate the necessity of redundant features, select pharmacophore points were systematically eliminated to generate four five-point and then four additional four-point pharmacophore models. The two aromatic and two hydrogen bond acceptor/metal ligator features (points 2, 3, 4, and 5) were hypothesized to chelate the divalent metals within the ATX active site,[40] although all four are unlikely to effectively chelate concurrently. Therefore, one or two of these points were removed to evaluate their optimal position. Four five-point pharmacophore models were generated, each lacking points 2, 3, 4, or 5 (Figure 3). Also, four four-point pharmacophores were generated, each lacking one aromatic and one hydrogen bond acceptor/metal ligator.

These nine pharmacophores were then each used to search the NCI open chemical repository database to prioritize screening efforts. Table 1 shows the distances measured among the pharmacophore points and the distance ranges used in subsequent database searches. Distance ranges were chosen by selecting ranges spanning 1 Å above and below the distance measured between pharmacophore points. If the virtual search yielded few or no hits then some ranges were expanded to generate less restrictive distance ranges, allowing for the identification of more virtual hits. Table 2 shows the number of compounds identified from searches using each pharmacophore model. Many compounds were identified by screens using multiple pharmacophore models. In all, 168 unique compounds were identified (Table 2). Of these 168 candidates, 106 compounds were acquired for subsequent screening (the remaining 62 compounds were no longer available).

All 106 compounds obtained from NCI were tested for autofluorescence (false negative), fluorescence quenching of carboxyfluorescein (false positive), and ATX inhibition using the FRET-based substrate FS-3. Autofluorescence (candidates alone) and fluorescence quenching (candidates plus 200 nM carboxyfluorescein) control screenings were done at single 10 μM concentrations of candidate inhibitors. One compound, **48** (2-(3-(phenylimino)-6-(4-sulfoanilino)-3*H*-xanthen-9-yl)benzoic acid, NSC[41] 11242, structure in Table S2 in the Supporting Information), showed autofluorescence equivalent to 15% of that of the 200 nM carboxyfluorescein control. No other

Table 2. Summary of Pharmacophore Performance

pharmacophore (points)	hits	hits acquired	actives	actives (%)	actives $IC_{50} < 1.5\,\mu M$	unique hits	unique actives	unique active (%)
6 (1, 2, 3, 4, 5, 6)	43	30	8	26.7	0	1	1	100
5a (1, 3, 4, 5, 6)	32	22	8	36.4	0	0	0	N/A
5b (1, 2, 4, 5, 6)	45	37	12	32.4	2	5	3	60.0
5c (1, 2, 3, 5, 6)	88	62	25	40.3	4	17	12	70.6
5d (1, 2, 3, 4, 6)	27	20	8	40.0	0	0	0	N/A
4a (1, 2, 3, 6)	43	30	11	36.7	1	0	0	N/A
4b (1, 2, 5, 6)	102	63	12	19.0	1	19	1	5.3
4c (1, 3, 4, 6)	34	24	9	37.5	0	0	0	N/A
4d (1, 4, 5, 6)	60	48	12	25.0	0	5	2	40.0

Table 3. Summary of the Characterization of Candidate ATX Inhibitors[a]

	pharmacophore									control screening				
candidate no.	6	5a	5b	5c	5d	4a	4b	4c	4d	false neg (%)[b]	false pos (%)[c]	ATX inhibition (%)[d]	IC_{50} (μM)	K_i (nM)[e]
1			X	X						0 ± 0	1 ± 1.4	93 ± 2.7	0.372 ± 0.051	270
2	X	X	X	X	X	X	X	X	X	0.7 ± 0.1	19 ± 1.3	84 ± 3.1	11.6	
3				X						0 ± 0	14 ± 1.3	82 ± 3.0	1.31	1890
4			X							1.7 ± 0.2	4 ± 1.4	80 ± 5.7	1.26	1460
5	X	X	X	X	X	X	X	X	X	1.1 ± 0.2	21 ± 1.3	80 ± 3.7	12.0	
6				X						0 ± 0	7 ± 1.4	77 ± 3.1	1.7	
7				X						0 ± 0	10 ± 1.3	76 ± 7.9	7.3	
8				X						0 ± 0	0 ± 1.4	75 ± 3.1	2.42 ± 0.588	
9				X						0 ± 0	4 ± 1.4	74 ± 3.2	5.4	
10						X	X			1.5 ± 0.2	3 ± 1.4	73 ± 2.8	0.805	1140
11									X	1.5 ± 0.2	14 ± 1.3	72 ± 3.7	8.9	
12	X	X	X	X	X	X	X	X	X	1.3 ± 0.2	27 ± 1.2	71 ± 3.6	11.6	
13		X	X	X	X	X	X	X	X	1.3 ± 0.1	26 ± 1.2	70 ± 4.9	13.8	
14				X						1.4 ± 0.2	13 ± 1.3	68 ± 5.5	13.4	
15				X						1.9 ± 0.2	4 ± 1.4	68 ± 2.6	5.9	
16		X	X	X	X	X	X	X	X	0.9 ± 0.1	17 ± 1.3	67 ± 3.7	18.6	
17				X						2.0 ± 0.2	7 ± 1.4	65 ± 2.9	ND[f]	
18				X		X			X	1.2 ± 0.2	20 ± 1.3	65 ± 2.9	15.5	
19			X							1.7 ± 0.2	8 ± 1.4	65 ± 2.9	28.1	
20				X						0 ± 0	3 ± 1.4	64 ± 4.9	0.922 ± 0.212	820
21				X		X	X		X	1.7 ± 0.2	16 ± 1.3	61 ± 3.8	19.1	
22									X	0 ± 0	2 ± 1.4	61 ± 2.9	7.8	
23	X	X	X	X	X	X	X	X	X	0 ± 0	11 ± 1.3	59 ± 4.3	18.2	
24				X						1.2 ± 0.2	3 ± 1.4	57 ± 3.8	17.4	
25	X			X			X			0 ± 0	−4 ± 1.3	55 ± 2.8	8.7	
26							X			0 ± 0	−1 ± 1.4	53 ± 7.2	7.4	
27			X							1.2 ± 0.2	6 ± 1.4	53 ± 3.7	37.6	
28	X									0 ± 0	7 ± 1.4	53 ± 3.7	7.6	
29				X						0.1 ± 0.0	15 ± 1.3	52 ± 5.6	9.8	
30	X	X		X				X		1.5 ± 0.2	18 ± 1.3	51 ± 6.1	12.6	
31				X						0 ± 0	0 ± 1.4	51 ± 4.6	9.3	
32	X	X	X	X	X	X	X	X	X	0 ± 0	−3 ± 1.4	49 ± 6.5	23.03	
33			X	X	X	X	X	X	X	0 ± 0	−4 ± 1.4	49 ± 4.4	ND[g]	

[a] Data for all active compounds (those that inhibited ATX activity by ≥50% at a single 10 μM concentration) are included. Data for inactive candidates is included in the Supporting Information. [b] False negative screening: candidate compounds were analyzed alone (excitation 485 nm, emission 520 nm) in assay buffer at 10 μM. Data are normalized to that of carboxyfluorescein (200 nM) in assay buffer. [c] False positive screening: candidate compounds were analyzed (excitation 485 nm, emission 520 nm) in assay buffer at 10 μM in the presence of carboxyfluorescein (200 nM). Data are presented as % inhibition of the carboxyfluorescein signal (200 nM). [d] ATX inhibition: single doses (10 μM) of candidate compounds tested against ATX (8.3 nM) with 1 μM FS-3. Data are normalized to vehicle control ATX-mediated FS-3 hydrolysis. [e] Mechanism of inhibition was determined using varying concentrations of FS-3 in the presence of three concentrations of candidate inhibitor (0, 0.5×, and 2× the IC_{50}). Simultaneous nonlinear regression of all data points was used to identify mechanism of inhibition and calculate K_i values. [f] ND: not determined. Because of the chemical instability of the trityl alcohol present in **17**, we have eliminated it from further characterization. [g] ND: not determined. The IC_{50} value for **33** could not be determined due to high curve fit errors.

candidate compounds produced more than 2% autofluorescence (Table 3 and Table S1 in the Supporting Information). Twelve of the 106 compounds showed modest quenching (15−30%) of the carboxyfluorescein fluorescent signal (Table 3 and Tables S2 and S3 in the Supporting Information). Compounds **5** (4-hydroxy-7-(3-(5-hydroxy-7-sulfo-6-((*E*)-(6-sulfonaphthalen-2-yl)diazenyl)naphthalen-2-yl)ureido)-3-((*E*)-*m*-tolyldiazenyl)naphthalene-2-sulfonic acid, NSC[41] 65574, Table S2), **12** (2-naphthalenesulfonic acid, {4-hydroxy-7-[[[[5-hydroxy-6-[(2-methylphenyl)azo]-7-sulfo-2-naphth}{alenyl]-amino]carbonyl]amino]-3-[(6-sulfo-2-naphthalenyl)azo]-} trisodium salt, NSC[41] 58057, Table S2), **13** (2-naphthalene sulfonic acid, {3[(4-amino-5-methoxy-2-}{methylphenyl)azo]-3′-[(6-sulfo-2-naphthyl)azo]-7,7′-}{(carbonyldiimino)bis[4-hydroxy-}

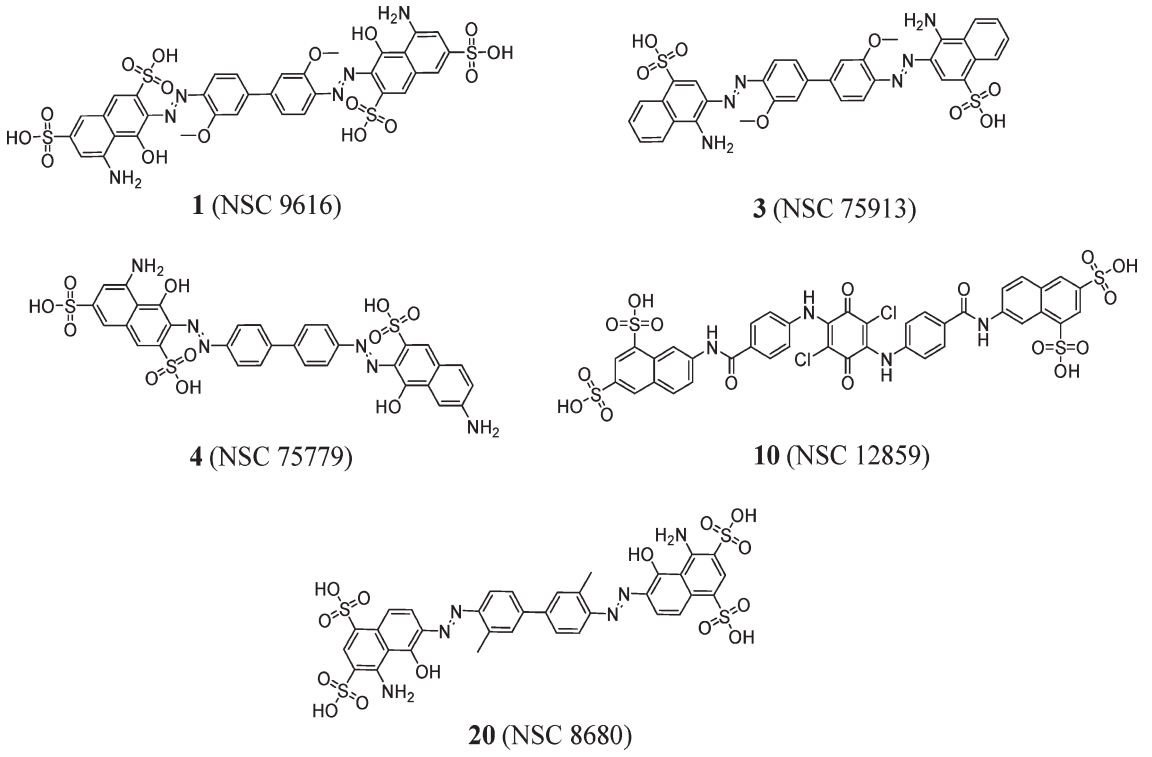

Figure 4. Structures for the five most potent ATX inhibitors.

trisodium salt, NSC[41] 58058, Table S2), and **41** (6,6′-((*E*)-ethene-1,2-diyl)bis(3-((*E*)-(2,4-diamino-5-methyl-3-((*E*)-(4-sulfophenyl)diazenyl)phenyl)diazenyl)benzenesulfonic acid), NSC[41] 65866, Table S2) showed false positive effects greater than 20% but were not among the most potent candidates examined. All compounds were then assayed at a single dose (10 μM) in the presence of purified recombinant human ATX (8.3 nM) and the synthetic ATX substrate FS-3 (1 μM). A 31% hit rate was achieved (33 out of the 106 compounds showed greater than 50% ATX inhibition at 10 μM), with **1** (5-amino-3-((4′-((8-amino-1-hydroxy-3,6-disulfo-2-naphthyl)diazenyl)-3,3′-dimethoxy[1,1′-biphenyl]-4-yl)diazenyl)-4-hydroxy-2,7-naphthalenedisulfonic acid, NSC[41] 9616, Figure 4) being the most efficacious as it inhibited ATX activity by 93 ± 2.7% (Table 3). Dose responses were acquired for 32 of 33 candidates showing greater than 50% ATX inhibition at this single dose (Table 3). Compound **17** (4-(4-((4-amino-3-methylphenyl)(4-anilinophenyl)hydroxymethyl)anilino)benzenesulfonic acid, NSC[41] 5014, Table S2) was eliminated from further consideration due to its chemically labile trityl alcohol functional group. Compound **1** was the most potent candidate identified with a determined IC_{50} of 372 ± 51 nM. Two other compounds showed nanomolar potency, **10** (7-((4-((2,5-dichloro-4-(4-(((6,8-disulfo-2-naphthyl)amino)carbonyl)anilino)-3,6-dioxo-1,4-cyclohexadien-1-yl)amino)benzoyl)amino)-1,3-naphthalenedisulfonic acid, NSC[41] 12859, Figure 4, IC_{50} = 805 nM) and **20** (NSC[41] 8680, Figure 4, IC_{50} = 922 ± 212 nM). Two additional compounds (**3** (4-amino-3-((4′-((1-amino-4-sulfo-2-naphthyl)diazenyl)-3,3′-dimethoxy[1,1′-biphenyl]-4-yl)diazenyl)-1-naphthalenesulfonic acid, NSC[41] 75913, Figure 4) and **4** (5-amino-3-((4′-((7-amino-1-hydroxy-3-sulfo-2-naphthyl)diazenyl)[1,1′-biphenyl]-4-yl)-diazenyl)-4-hydroxy-2,7-naphthalenedisulfonic acid, NSC[41] 75779, Figure 4)) were also determined to have low micromolar potency with IC_{50} values of 1.31 and 1.26 μM, respectively. Structures for all active and inactive candidates evaluated can be found in Table S2 of the Supporting Information. The raw data used to plot dose response curves can be found in Table S4 of the Supporting Information.

Table 4. Experimentally Determined Mechanism of ATX Iinhibition and K_i and Values for the Six Most Potent Candidates

compd	K_i (μM)	mechanism
1	0.271	competitive
3	1.89	noncompetitive
4	1.46	competitive
10	1.14	competitive
20	0.824	competitive

The mechanism of ATX inhibition was determined for the five most potent candidates, those with $IC_{50} \leq 1.5$ μM (Table 4). Compound **3** demonstrated noncompetitive inhibition, where affinity for free enzyme and the enzyme−substrate complex are equal. Here K_i and K_i' were equal to 1.89 μM (Table 4). Compounds **1**, **4**, **10**, and **20** showed competitive inhibition with K_i values equal to 0.271, 1.46, 1.14, and 0.824 μM, respectively. These compounds have a preference for the free enzyme over the enzyme substrate complex. The FS-3 and inhibitor concentrations and initial velocities can be found in Table S5 of the Supporting Information.

In addition to the synthetic substrate, FS-3, we also examined inhibition of ATX activity using the endogenous substrate, LPC (16:0), in a choline release assay. This assay proved problematic as a screening tool for ATX inhibitor discovery. Figure 5 shows data for a subset of the candidates also characterized using ATX-mediated FS-3 hydrolysis. Several compounds, including **36** (7-((4-((4-aminobenzoyl)amino)benzoyl)amino)-4-hydroxy-2-naphthalenesulfonic acid, NSC[41] 1741, Table S2), **60** (2-((1-(4-(2-(4-(((4-(2-(4-(4-((2-carboxyphenyl)diazenyl)-3-methyl-5-oxo-4,5-dihydro-1*H*-pyrazol-1-yl)-2-sulfophenyl)-vinyl)-3-sulfoanilino)carbonyl)amino)-2-sulfophenyl)vinyl)-3-sulfophenyl)-3-methyl-5-oxo-4,5-dihydro-1*H*-pyrazol-4-yl)diazenyl)benzoic acid, NSC[41] 34937, Table S2), **64** (rhoduline

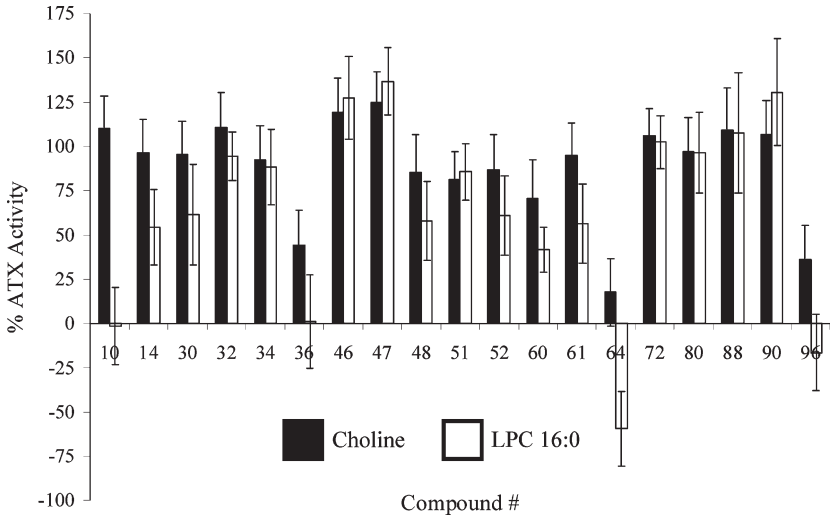

Figure 5. Compound screening utilizing either the natural ATX substrate LPC 16:0 (open bars) or the product choline (closed bars) and the choline release assay components. Data are mean ± SD of triplicate samples.

acid, NSC[41] 1698, Table S2), and **96** (8-((4-(((4-(((3,8-disulfo-1-naphthyl)amino)carbonyl)anilino)carbonyl)amino)benzoyl)-amino)-1,6-naphthalenedisulfonic acid, NSC[41] 12188, Table S2), show significant false positive effects in the presence of choline and the choline release assay components. These compounds, therefore, show greater effect on apparent ATX activity in the presence of the substrate LPC (16:0) due to interference with either choline release assay component(s) or fluorescence quenching. No further efforts were made to screen or characterize ATX inhibitors using this assay.

To address selectivity, the five most potent candidate ATX inhibitors were also tested for their ability to inhibit NPP6 and NPP7, the only other NPP isoforms with currently identified preferences for lipid substrates.[42,43] None of these compounds showed false negative or positive effects as determined by absorbance at 405 nm in the absence or presence of *p*-nitrophenol, the product of NPP6/7-mediated hydrolysis of the synthetic substrate, *para*-nitrophenylphosphocholine (pNPPC), data shown in Supporting Information, Table S3. In addition, none of the five candidates had a significant effect on NPP6-mediated hydrolysis of pNPPC (Supporting Information, Table S3). Likewise, compounds **1**, **3**, **4**, and **20** failed to inhibit NPP7-mediated hydrolysis of pNPPC, although compound **10** modestly inhibited NPP7 by ~20% (Supporting Information, Table S3).

Discussion

Pharmacophore modeling is useful in identifying the types and relative locations of functional groups required to produce a desired biological response. Structure-based and ligand-based approaches are used to generate pharmacophore models.[44] Structure-based pharmacophore modeling utilizes the complex between a ligand and its biological target as a starting point, whereas ligand-based pharmacophore modeling employs the ligand in a putative active conformation as template.[44] Structure-based pharmacophore models for ATX are currently problematic, as knowledge of the three-dimensional structure of the enzyme active site is limited due to a lack of X-ray crystal or NMR data. Thus, a ligand-based pharmacophore approach was chosen for this work, given that there is a growing list of published ATX inhibitors, including both lipid[25−33,35] and nonlipid examples.[36−38] For these studies, we elected not to use published lipid-like ATX inhibitors for our pharmacophore models due to the high degree of flexibility within these structures, which would make selection of a putative bioactive conformation very difficult in the absence of enzyme-derived constraints. The nonlipid compounds identified previously by Parrill and colleagues are substantially less flexible, thus allowing determination of a conformation for each that places common chemical functionality within overlapping volumes.[37]

Structure-based pharmacophore models have previously been generated for a variety of biological targets. Although we do not have the benefit of a complex between ATX and an inhibitor, we hypothesized that a subset of four pharmacophore points (2, 3, 4, and 5) could chelate one of two divalent metal cations within the enzyme active site. We have shown that inclusion of the aromatic functional group (point 3) has a profound effect on the ability to identify active ATX inhibitors and might therefore be optimally placed for metal chelation. Recently, a structure-based pharmacophore was developed for 11β-hydroxysteroid dehydrogenase.[45] In this study, two pharmacophore models were developed from the target cocrystallized with a synthetic inhibitor to evaluate the position of a hydrogen bond acceptor in one of two positions (interaction between one of two protein residues, S170 and Y183) using virtual screening.[45] This approach allowed the identification of 11 new 11β-hydroxysteroid dehydrogenase inhibitors with IC_{50} values less than 10 μM.[45] Seven of the 11 identified inhibitors had a hydrogen bond acceptor that was able to interact with S170 and Y183. These dual interacting compounds were more potent than the other four, which interacted with only S170.[45] Despite using a ligand-based rather than a structure-based approach, we were able to identify the aromatic pharmacophore point 3 as being optimally placed for interaction with ATX, perhaps by metal chelation based on previous knowledge of the proposed ATX catalytic cycle.[40] Inclusion of feature 3 contributed to the identification of four out of the five most potent ATX inhibitors identified herein.

Ligand-based pharmacophore development using conformational analysis of known ligands has also been used in a variety of biological systems and is most widely utilized when the biological target or structure is unknown. Here we developed pharmacophore models from a flexible alignment of

previously identified nonlipid ATX inhibitors in an effort to identify common functional group features and to define distance ranges that describe their three-dimensional relationship. These data were then utilized to search an online chemical database to identify nonlipid ATX inhibitors. In a different system, a ligand-based pharmacophore was developed for the CXCR4 chemokine receptor to identify new nonpeptide antagonists.[46] Previously identified cyclic peptide antagonists, with the backbone held rigid, were subjected to conformational analysis.[46] Rather than virtual database mining, distance ranges among the key residues required for CXCR4 antagonist activity were measured to identify a new core using rational drug design.[46] This study focused on the development of nonpeptide antagonists that utilized amino acid side chain functional groups such as aromatic and guanidine groups.[46] Their system required inclusion of specific functional groups where database mining was unlikely to uncover significant numbers of hits, therefore a rational de novo design was employed to identify a nonpeptide core.[46] Because our system had no such limitations of functional groups, we searched an online database with adaptable functional groups where the core of our hits could vary. These criteria made our system more tractable for a virtual screening approach.

The phosphate functional group is commonly modified via bioisosteric replacement due to the susceptibility of endogenous and exogenous organic phosphates to metabolism by biologically relevant phosphatases and phosphodiesterases. Both the natural ATX substrate, LPC, and the endogenous ATX feedback inhibitor, LPA, contain phosphate groups.[25] The majority of nonlipid ATX inhibitors utilized to define the pharmacophore models contain carboxylic acids, one classical phosphate bioisostere.[47] Additional phosphate bioisosteres include sulfates, phosphosphonates, α-halogenated phosphonates, sulfonic acids, α-halogenated sulfonic acids, and α-halogenated carboxylic acids.[48−50] These features are functionally interchangeable due to their ability to adopt a negative charge at biological pH. The most effective ATX inhibitors identified to date have at least one anionic functional group, Figure 1.[36,37] Sulfonic acids are well represented in the NCI open chemical repository database. Therefore, we chose this as the anionic isostere in our initial screens. Sulfonic acid containing compounds have been shown here to mediate successful interactions with ATX via the identification of 33 active nonlipid compounds, validating our expectation that a broad variety of anionic groups can serve in place of phosphate or carboxylate features in ATX inhibitors.

Pharmacophore 6 identified active ATX inhibitors at a rate of 26.7% (Table 2 and Figure 6). These rates increased to between 32.4 and 40.0% when a single feature was removed in the five-point models (5a−d). However, upon removal of a second feature, hit rates were either unchanged or significantly worse (ranging from 19.0 to 37.5%) in the four-point models (4a−d). These data suggest that the six-point model is too restrictive but that elimination of two features can be detrimental. It is apparent that pharmacophores 5c and 4b generated the greatest numbers of total hits, 62 and 63, respectively. However, a significantly greater number of the active inhibitors were identified by model 5c (25 of 33 total active compounds, 75.8%) than by model 4b (12 of 33 actives, 36.4%). A total of 13 of 33 active candidates (39.4%) were identified by model 5c but not model 4b, including three of the most potent compounds (**1**, **3**, and **20**). In contrast, only 2 of 33 active candidates (6.1%) were identified by model 4b but not model 5c, including one of the most potent compounds (**10**). In addition, a smaller portion of inactive compounds were identified by model 5c (37 of 73 inactive hits, 50.7%) than model 4b (51 of 73, 69.9%), see Table S1 in the Supporting Information. Within the inactive compounds, model 5c incorrectly labeled only six compounds as active that were not also identified by model 4b. These data suggest application of a two-step screening process by which searches are conducted with pharmacophores 5c and 4b and compounds identified by 5c but not 4b are carried forward for subsequent analysis.

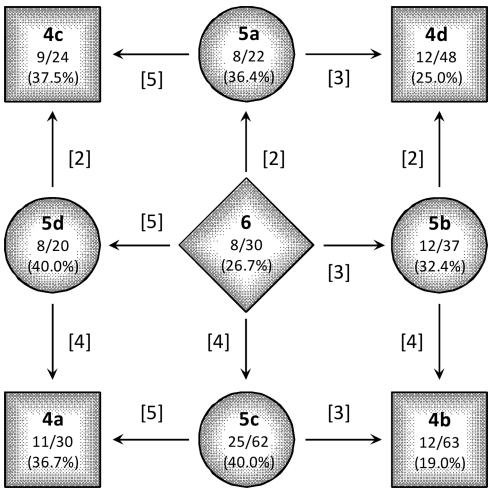

Figure 6. Illustrative comparison of the nine pharmacophore models. Bold numbers represent the number of pharmacophore points represented in each model. Fractional numbers represent the number of actives/total number of hits for that model (percent hits). The number in brackets shows which pharmacophore feature has been removed to generate the subsequent model.

ATX is a metalloenzyme that requires two divalent metal cations and a single catalytic residue, T210, for enzymatic activity.[51,52] In 2005, it was shown that metal chelators, like L-histidine, inhibited ATX hydrolytic activity at millimolar concentrations.[53] In our study, we have utilized the strategy of metal chelation by small molecules in order to inhibit ATX. Pharmacophore points 2, 3, 4, and 5 are all potential metal chelators. Pharmacophore points 2 and 4 were modeled as oxygen for its ability to act as either a hydrogen bond acceptor or a metal chelator. Pharmacophore points 3 and 5 are aromatic functional groups that have the ability to engage in cation−π interactions involving the delocalized electrons in the aromatic ring and divalent metal cations. Out of the eight pharmacophores (4a−d and 5a−d) that probe the location of the metal chelating features, models lacking point 3 have significantly lower hit rates (Table 2). Pharmacophore models 4b and 4d, each lacking point three, have hit rates of 19.0 and 25.0%, compared to 4a and 4c with hit rates of 36.7 and 37.5%. Pharmacophore 5b (lacking point 3), has the lowest hit rate among all of the five-point models. This suggests that pharmacophore point 3 is required for optimal ATX interaction, perhaps through metal chelation.

Pharmacophore models that include points 1, 3, and 6 span an increased overall length and had improved hit rates. Pharmacophore 4b had the lowest hit rate among all the pharmacophore models (19.0%) and the shortest overall length (11.96 Å). The other four-point pharmacophore models achieved significantly higher hit rates from 25.0 to 37.5%. Inclusion of pharmacophore point 3 created the longest pharmacophore (the distance from points 1−3 is 15.04 Å)

and resulted in higher hit rates, suggesting longer overall compounds are preferred to inhibit ATX. A similar trend has been noted in the evaluation of LPC structure−activity relationships with ATX, where short-chained LPC compounds were less effective whether they were tested as substrates[2] or as inhibitors.[54] These results suggest that very small molecules may not occupy enough of the ATX active site to effectively block enzymatic activity.

The candidate ATX inhibitors identified here in our initial pharmacophore searches have expanded the diversity of established ATX inhibitors (Figure 4). Here we report the first sulfonic acid ATX inhibitors. These new nonlipid ATX inhibitors clearly exhibit ATX activity in vitro, and are strong candidates for further evaluation in cellular and in vivo assays.

Experimental Section

Pharmacophore Development and Database Screening. Eight previously identified, small molecule ATX inhibitors[37] were built using MOE[39] and ionized as predicted at biological pH. Flexible alignment to identify the three-dimensional arrangement of structural features common to all eight examples was also performed in MOE using default settings with the exception that the acid/base parameter was enabled and the MMFF94[55] force field was used to assign partial charges. From a total of 25 flexible alignments, the optimum was chosen visually by selecting that alignment containing maximal molecular overlap (shared common volume) for all eight inhibitors. The pharmacophore points (one anionic group, one hydrogen bond donor, two hydrogen bond acceptors/metal ligators, and two aromatic groups) were identified as those structural features within at least five of eight inhibitors sharing common volumes. The following functional groups, sulfonic acid (anion, point 1), phenyl (aromatic, points 3 and 5), oxygen (hydrogen bond acceptor/metal ligator, points 2 and 4), and N−H (hydrogen bond donor, point 6) were used for online searches of the NCI open chemical repository. Unfortunately, the NCI database interface limits the total number of distance constraints to six, which is insufficient to completely describe the three-dimensional relationship between all the pharmacophore points in the five-point and six-point pharmacophore models. The distances utilized and the ranges used for each search are shown in Table 1. The default settings were used for all online searches with the exception of the hit limit, which was extended to 1000. If searches reached either the hit or time limit, the search was repeated in discrete molecular weight ranges (up to 4000 g/mol) to ensure the whole NCI database was searched. A total of 168 compounds that matched one or more of the nine pharmacophore searches were identified and requested. A total of 106 compounds were available and were screened as ATX inhibitors.

ATX (NPP2) Expression and Purification. A mammalian expression vector, pCMV5, containing the human ATX sequence with a C-terminal FLAG affinity tag was a generous gift from Professor Junken Aoki (Tohoku University, Aoba-ku, Sendai, Japan). This construct was subsequently subcloned into the pFastBac1 transfer vector between *Bam*HI and *Hin*dIII sites using standard molecular biology techniques. Bacmid and viral stock were prepared using the bac-to-bac Baculovirus Expression System (Invitrogen, Carlsbad, CA) according to the manufacturer's protocol. ATX protein was expressed in 1 L Sf9 insect cell cultures (2×10^6 cells mL^{-1}) in Sf-900 III serum free media (Invitrogen, Carlsbad, CA). Cells were infected with 10 mL of high titer virus stock at 27 °C for 72 h. Soluble ATX present in the medium was clarified via centrifugation at 3000*g* with subsequent affinity purification of the supernatant using anti-FLAG M2 agarose (Sigma Aldrich, St. Louis, MO). After removing nonspecifically bound proteins using TBS buffer (50 mM Tris HCl and 150 mM NaCl at pH 7.4), ATX was eluted using TBS buffer containing FLAG peptide (50 μg/mL, Sigma Aldrich, St. Louis, MO).

NPP6 Expression and Purification. A mammalian expression vector, pCAGGS-MCS, containing the human NPP6 sequence was a generous gift from Dr. Junken Aoki (University of Tokyo, Tokyo, Japan). A C-terminal FLAG affinity tag was incorporated at position 419 and a stop codon included downstream of the FLAG-tag. This construct was subcloned into the pFastBac1 transfer vector between *Eco*RI and *Xho*I sites using standard molecular biology techniques. Bacmid and viral stock were prepared using the bac-to-bac Baculovirus Expression System (Invitrogen, Carlsbad, CA) according to the manufacturer's protocol. NPP6 was expressed in 1 L Sf9 insect cell cultures (2×10^6 cells mL^{-1}) in Sf-900 III SFM serum free media (Invitrogen, Carlsbad, CA). Cells were infected with 10 mL of high titer virus stock and incubated at 27 °C for 48 h. Soluble NPP6 present in the medium was clarified via centrifugation at 3000*g* with subsequent affinity purification of the supernatant using anti-FLAG M2 agarose (Sigma Aldrich, St. Louis, MO). After removing nonspecifically bound proteins using TBS buffer, NPP6 was eluted using TBS buffer containing FLAG peptide (50 μg/mL, Sigma Aldrich, St. Louis, MO).

NPP7 Expression and Purification. A mammalian expression vector, pcDNA4/TO/myc His B, containing the human NPP7 sequence was a generous gift from Dr. Rui Dong-Duan (Lund University, Lund, Sweden). A C-terminal FLAG affinity tag was incorporated at position 415 and a stop codon included downstream of the FLAG-tag. This construct was subcloned into the pFastBac1 transfer vector between *Bam*HI and *Not*I sites using standard molecular biology techniques. Bacmid and viral stock were prepared using the bac-to-bac Baculovirus Expression System (Invitrogen, Carlsbad, CA) according to the manufacturer's protocol. NPP7 was expressed in 1 L Sf9 insect cell cultures (2×10^6 cells mL^{-1}) in Sf-900 III SFM serum free media (Invitrogen, Carlsbad, CA). Cells were infected with 10 mL of high titer virus stock and incubated at 27 °C for 72 h. Soluble NPP7 present in the medium was clarified via centrifugation at 3000*g* with subsequent affinity purification of the supernatant using anti-FLAG M2 agarose (Sigma Aldrich, St. Louis, MO). After removing nonspecifically bound proteins using TBS buffer, NPP7 was eluted using TBS buffer containing FLAG peptide (50 μg/mL, Sigma Aldrich, St. Louis, MO).

Screening Assays. The top five most potent ATX inhibitors (Table 4) were determined to be ≥95% pure by reverse-phase HPLC.

FS-S-Based Screening. Autofluorescence (false negative screening) was monitored by incubating the ATX inhibitor candidate (final concentration 10 μM) in assay buffer (1 mM $MgCl_2$, 1 mM $CaCl_2$, 3 mM KCl, 140 mM NaCl, 50 mM Tris, pH 8) and 30 μM bovine serum albumin (BSA) at 37 °C. Data were reported as percent of a separate carboxyfluorescein control (200 nM). All data were reported as a mean ± standard deviation of three wells.

False positive screening to determine fluorescence quenching was performed by combining ATX inhibitor candidates (final concentration 10 μM) with carboxyfluorescein (final concentration 200 nM) in the presence of fatty acid free BSA (final concentration 30 μM) in assay buffer (1 mM $MgCl_2$, 1 mM $CaCl_2$, 3 mM KCl, 140 mM NaCl, 50 mM Tris, pH 8). Data were reported as percent reduction relative to a separate carboxyfluorescein control (200 nM). All data were reported as a mean ± standard deviation of three wells.

ATX inhibition was monitored using the synthetic fluorescent substrate FS-3 (Echelon Biosciences, Inc., Salt Lake City, UT), purified recombinant human ATX, and inhibitor, each of which constitutes a third of the total volume. Final concentrations on the plate were 1 μM for FS-3 and 30 μM for fatty acid free bovine serum albumin, both of which were dissolved in assay buffer (1 mM $MgCl_2$, 1 mM $CaCl_2$, 3 mM KCl, 140 mM NaCl, 50 mM Tris, pH 8). Single dose final inhibitor concentrations

were 10 μM. For dose responses, final inhibitor concentrations were 30, 10, 3, 1, 0.3, 0.1, and 0.03 μM, except for **1**, **3**, **4**, **10**, and **20**, where two extra concentrations (0.01 and 0.003 μM) were used in assay buffer. The final concentration of purified ATX on the plate was 8.3 nM. All assays were carried out in 96-well, half area plates (Corning Inc., Corning, NY) at 37 °C in a BioTek Synergy-2 plate reader (BioTek, Winooski, VT) with excitation and emission wavelengths of 485 and 538 nM, respectively. Data points were collected every 2 min and are reported as percent ATX activity with respect to vehicle control after subtraction of fluorescence with no ATX, at the 1 h time point. The fluorescent signal with respect to time was linear out to the 1 h time point. All data were reported as a mean ± standard deviation of three wells. All dose response data was validated within 10% except for **1**, **8**, and **20**, for which standard deviation is reported.

LPC/Amplex Red-Based Screening. False positive screening was carried out using Amplex Red cocktail consisting of choline oxidase (0.1 U/mL), horseradish peroxidase (1 U/mL), and the Amplex Red reagent (10 μM), where concentrations reported are final concentrations. Final concentrations of the ATX inhibitor candidate and choline oxidase substrate (choline) were 10 and 1 μM, respectively. All assays were run in the presence of fatty acid free BSA (final concentration 30 μM) in assay buffer (50 mM Tris, 5 mM $CaCl_2$, pH 7.4). All data, mean ± standard deviation of three wells, are reported as percent of choline control.

ATX inhibition was also monitored using the Amplex Red reagent (Invitrogen, Carlsbad, CA), purified recombinant human ATX, and inhibitor, each of which constitutes a third of the total volume. The Amplex Red cocktail consisted of choline oxidase (0.1 U/mL), horseradish peroxidase (1 U/mL), and the Amplex Red reagent (10 μM), where concentrations reported are final concentrations. Final concentrations of the ATX inhibitor candidate and substrate (LPC 16:0) were 10 and 100 μM, respectively. All assays were run in the presence of fatty acid free BSA (final concentration 30 μM) in assay buffer (50 mM Tris, 5 mM $CaCl_2$, pH 7.4). The final concentration of purified ATX was 8.3 nM. All assays were carried out in 96-well, half-area plates (Corning Inc., Corning, NY) at 37 °C in a BioTek Synergy-2 plate reader (BioTek, Winooski, VT) with excitation and emission wavelengths of 560 and 590 nM, respectively. Data points were collected every 2 min and are reported as percent ATX activity with respect to vehicle control after subtraction of fluorescence with no ATX, at the 1 h time point. The fluorescent signal with respect to time was linear past the 1 h time point. All data was reported as a mean ± standard deviation of three wells.

Mechanism of Inhibition. Mechanism of ATX inhibition was identified by incubating three concentrations of the ATX inhibitor candidate with varying concentrations of substrate (FS-3). The final concentrations of inhibitors used were zero, one-half, and twice the experimentally determined IC_{50}. The final concentrations of FS-3 used ranged from 0.3 to 20 μM. All assays were run in the presence of fatty acid free BSA (final concentration 30 μM) in assay buffer (1 mM $MgCl_2$, 1 mM $CaCl_2$, 3 mM KCl, 140 mM NaCl, 50 mM Tris, pH 8). All assays were carried out in 96-well, half-area plates (Corning Inc., Corning, NY) at 37 °C in a BioTek Synergy-2 plate reader (BioTek, Winooski, VT) with excitation and emission wavelengths of 485 and 538 nM, respectively. Data were reported as the mean of three wells and plotted on a logarithmic scale. All data points were curve fitted with Michealis−Menton equations for competitive, uncompetitive, mixed-mode, and noncompetitive inhibition using simultaneous nonlinear regression for each model using WinNonLin 6.1 (Pharsight, Mountain View, CA). Mechanism of inhibition was assigned by determining the lowest averaged percent residuals for each mechanism. K_i and K_i' values represent compound affinity for free enzyme and the enzyme−substrate complex, respectively. Initial rates for the zero inhibitor concentration were plotted against the substrate concentration, and a rectangular hyperbolic curve was fitted to the data using KaleidaGraph (version 4.03, Synergy Software, Reading, PA) to determine K_m. The average K_m for ATX-mediated FS-3 hydrolysis was determined to be 3.4 ± 1.0 μM ($n = 6$) in our hands and was used in the following calculations.

For competitive inhibition:

$$V_o = \frac{V_{max}[S]}{\alpha K_m + [S]} \text{ where } \alpha = 1 + \frac{[I]}{K_i}$$

For uncompetitive inhibition:

$$V_o = \frac{V_{max}[S]}{K_m + \alpha'[S]} \text{ where } \alpha' = 1 + \frac{[I]}{K_i'}$$

For mixed-mode inhibition:

$$V_o = \frac{V_{max}[S]}{\alpha K_m + \alpha'[S]}$$

For noncompetitive inhibition ($\alpha = \alpha'$), therefore:

$$V_o = \frac{V_{max}[S]}{\alpha(K_m + [S])}$$

Candidate Specificity, NPP6/7 Inhibition. NPP6/7 inhibition was monitored using the synthetic absorbance substrate *para*-nitrophenylphosphocholine (pNPPC) (Sigma Aldrich, St. Louis, MO), purified recombinant human NPP6/7, and inhibitor candidate, each of which constituted one-third of the total volume. Final concentrations of pNPPC on the plate were 10 μM for NPP6 and 500 μM for NPP7. Final concentrations of inhibitor candidate and enzyme (NPP6/7) were 10 μM and 8.3 nM, respectively. All materials were dissolved in assay buffer. The assay buffer for the NPP6 assays consisted of 500 mM NaCl, 100 mM Tris-HCl, and 0.05% Triton X-100 at pH 9.[43] The assay buffer used for the NPP7 assays consisted of 50 mM Tris HCl, 150 mM NaCl, and 10 mM sodium taurocholate at pH 8.[42] All assays were carried out in 96-well, half-area plates (Corning Inc., Corning, NY) at 37 °C in a BioTek Synergy-2 plate reader (BioTek, Winooski, VT) with absorbance monitoring at 405 nM. Data points were collected every 2 min and are reported as percent enzyme activity with respect to vehicle control after subtraction of absorbance with no enzyme, at the 1 h time point. The absorbance signal with respect to time was linear past the 1 h time point. All data were reported as a mean ± standard deviation of three wells.

Acknowledgment. We thank the Chemical Computing Group for supplying the University of Memphis, Department of Chemistry, with MOE. We also thank The NCI/DTP Open Chemical Repository (http://dtp.cancer.gov) for all of the compounds tested. Finally, we thank Dr. Junken Aoki for the NPP2 and NPP6 plasmids and Dr. Ruin Dong-Duan for the NPP7 plasmid.

Supporting Information Available: Characterization of inactive ATX inhibitor candidates, structures for all compounds, and NPP6/7 inhibition results for compounds **1**, **3**, **4**, **10**, and **20**. This material is available free of charge via the Internet at http://pubs.acs.org.

References

(1) Stracke, M.; Krutzch, H.; Unsworth, E.; Arestad, A.; Cioce, V.; Schiffmann, E.; Liotta, L. Identification, purification, and partial sequence analysis of autotaxin, a novel motility-stimulating protein. *J. Biol. Chem.* **1992**, *267*, 2524–2529.

(2) Tokumura, A.; Majima, E.; Kariya, Y.; Tominaga, K.; Kogure, K.; Yasuda, K.; Fukuzawa, K. Identification of human plasma lysophospholipase D, a lysophosphatidic acid-producing enzyme, as autotaxin, a multifunctional phosphodiesterase. *J. Biol. Chem.* **2002**, *277*, 39436–39442.

(3) Umezu-Goto, M.; Kishi, Y.; Taira, A.; Hama, K.; Dohmae, N.; Takio, K.; Yamori, T.; Mills, G.; Inoue, K.; Aoki, J.; Arai, H.

Autotaxin has lysophospholipase D activity leading to tumor cell growth and motility by lysophosphatidic acid production. *J. Cell Biol.* **2002**, *158*, 227–233.
(4) Mills, G. a. M., W. The emerging role of lysophosphatidic acid in cancer. *Nature Rev. Cancer* **2003**, *3*, 582–591.
(5) Tabata, K.-i.; Baba, K.; Shiraishi, A.; Ito, M.; Fujita, N. The orphan GPCR GPR87 was deorphanized and shown to be a lysophosphatidic acid receptor. *Biochem. Biophys. Res. Commun.* **2007**, *363*, 861–866.
(6) Parrill, A. L. Lysophospholipid interactions with protein targets. *Biochim. Biophys. Acta* **2008**, *1781*, 540–546.
(7) Pasternack, S. M.; von Kugelgen, I.; Aboud, K. A.; Lee, Y.-A.; Ruschendorf, F.; Voss, K.; Hillmer, A. M.; Molderings, G. J.; Franz, T.; Ramirez, A.; Nurnberg, P.; Nothen, M. M.; Betz, R. C. G protein-coupled receptor P2Y5 and its ligand LPA are involved in maintenance of human hair growth. *Nat. Genet.* **2008**, *40*, 329–334.
(8) Lee, C.-W.; Rivera, R.; Gardell, S.; Dubin, A. E.; Chun, J. GPR92 as a new G12/13, and Gq, coupled lysophosphatidic acid receptor that increases cAMP, LPA5. *J. Biol. Chem.* **2006**, *281*, 23589–23597.
(9) Murakami, M.; Shiraishi, A.; Tabata, K.; Fujita, N. Identification of the orphan GPCR, $P2Y_{10}$ receptor as the sphingosine-1-phosphate and lysophosphatidic acid receptor. *Biochem. Biophys. Res. Commun.* **2008**, *371*, 707–712.
(10) van Meeteren, L. A.; Moolenaar, W. H. Regulation and biological activities of the autotaxin-LPA axis. *Prog. Lipid Res.* **2007**, *46*, 145–160.
(11) Stassar, M. J.; Devitt, G.; Brosius, M.; Rinnab, L.; Prang, J.; Schradin, T.; Simon, J.; Petersen, S.; Kopp-Schneider, A.; Zoller, M. Identification of human renal cell carcinoma associated genes by suppression subtractive hybridization. *Br. J. Cancer* **2001**, *85*, 1372–1382.
(12) Debies, M. T.; Welch, D. R. Genetic basis of human breast cancer metastasis. *J. Mammary Gland Biol. Neoplasia* **2001**, *6*, 441–451.
(13) Euer, N.; Schwirzke, M.; Evtimova, V.; Burtscher, H.; Jarsch, M.; Tarin, D.; Weidle, U. H. Identification of genes associated with metastasis of mammary carcinoma in metastatic versus non-metastatic cell lines. *Anticancer Res.* **2002**, *22*, 733–740.
(14) Yang, S. Y.; Lee, J.; Park, C. G.; Kim, S.; Hong, S.; Chung, H. C.; Min, S. K.; Han, J. W.; Lee, H. W.; Lee, H. Y. Expression of autotaxin (NPP-2) is closely linked to invasiveness of breast cancer cells. *Clin. Exp. Metastasis* **2002**, *19*, 603–608.
(15) Kehlen, A.; Englert, N.; Seifert, A.; Klonisch, T.; Dralle, H.; Langner, J.; Hoang-Vu, C. Expression, regulation and function of autotaxin in thyroid carcinomas. *Int. J. Cancer* **2004**, *109*, 833–838.
(16) Kishi, Y.; Okudira, S.; Kishi, M.; Hama, K.; Shida, D.; Kitayama, J.; Yamori, T.; Aoki, J.; Fujimaki, T.; Arai, H. Autotaxin is overexpressed in glioblastoma multiforme and contributes to cell motility of glioblastoma by converting lysophosphatidylcholine to lysophosphatidic acid. *J. Biol. Chem.* **2006**, *281*, 17492–17500.
(17) Hoelzinger, D. B.; Mariani, L.; Weis, J.; Woyke, T.; Berens, T. J.; McDonough, W. S.; Sloan, A.; Coons, S. W.; Berens, M. E. Gene expression profile of glioblastoma multiforme invasive phenotype points to new therapeutic targets. *Neoplasia* (*New York*) **2005**, *7*, 7–16.
(18) Ferry, G.; Giganti, A.; Coge, F.; Bertaux, F.; Thiam, K.; Boutin, J. A. Functional invalidation of the autotaxin gene by a single amino acid mutation in mouse is lethal. *FEBS Lett.* **2007**, *581*, 3572–3578.
(19) Tanaka, M.; Okudaira, S.; Kishi, Y.; Ohkawa, R.; Iseki, S.; Ota, M.; Noji, S.; Yatomi, Y.; Aoki, J.; Arai, H. Autotaxin stabilizes blood vessels and is required for embryonic vasculature by producing lysophosphatidic acid. *J. Biol. Chem.* **2006**, *281*, 25822–25830.
(20) van Meeteren, L.; Ruurs, P.; Stortelers, C.; Bouwman, P.; van Rooijen, M.; Pradere, J.; Pettit, T.; Wakelam, M.; Saulnier-Blache, J.; Mummery, C.; Moolenaar, W.; Jonkers, J. Autotaxin, a secreted phospholipase D, is essential for blood vessel formation during development. *J. Biol. Chem.* **2006**, *26*, 5015–5022.
(21) Umemura, K.; Yamashita, N.; Yu, X.; Arima, K.; Asada, T.; Makifuchi, T.; Murayama, S.; Saito, Y.; Kanamaru, K.; Goto, Y.; Kohsaka, S.; Kanazawa, I.; Kimura, H. Autotaxin expression is enhanced in frontal cortex of Alzheimer-type dementia patients. *Neurosci. Lett.* **2006**, *400*, 97–100.
(22) Zhao, C.; Fernandes, M. J.; Prestwich, G. D.; Turgeon, M.; Battista, J. D.; Clair, T.; Poubelle, P. E.; Bourgoin, S. G. Regulation of lysophosphatidic acid receptor expression and function in human synoviocytes: Implications for rheumatoid arthritis? *Mol. Pharmacol.* **2008**, *73*, 587–600.
(23) Boucher, J.; Quilliot, D.; Pradere, J.-P.; Simon, M.-F.; Gres, S.; Guigne, C.; Prevot, D.; Ferry, G.; Boutin, J. A.; Carpene, C.; Valet, P.; Saulnier-Blache, J. S. Potential involvement of adipocyte insulin resistance in obesity-associated up-regulation of adipocyte lysophospholipase D/autotaxin expression. *Diabetologia* **2005**, *48*, 569–577.
(24) Inoue, M.; Ma, L.; Aoki, J.; Chun, J.; Ueda, H. Autotaxin, a synthetic enzyme of lysophosphatidic acid (LPA), mediates the induction of nerve-injured neuropathic pain. *Mol. Pain* **2008**, 4.
(25) van Meeteren, L.; Ruurs, P.; Christodoulou, E.; Goding, J.; Takakusa, H.; Kikuchi, K.; Perrakis, A.; Nagano, T.; Moolenaar, W. Inhibition of autotaxin by lysophosphatidic acid and sphingosine 1-phosphate. *J. Biol. Chem.* **2005**, *280*, 21155–21161.
(26) Zhang, H.; Xu, X.; Gajewiak, J.; Tsukahara, R.; Fujiwara, Y.; Liu, J.; Fells, J.; Perygin, D.; Parrill, A. L.; Tigyi, G.; Prestwich, G. D. Dual activity lysophosphatidic acid receptor pan-antagonist/autotaxin inhibitor reduces breast cancer cell migration in vitro and causes tumor regression in vivo. *Cancer Res.* **2009**, *69*, 5441–5449.
(27) Cui, P.; Tomsig, J. L.; McCalmont, W. F.; Lee, S.; Becker, C. J.; Lynch, K. R.; Macdonald, T. L. Synthesis and biological evaluation of phosphonate derivatives as autotaxin (ATX) inhibitors. *Bioorg. Med. Chem. Lett.* **2007**, *17*, 1634–1640.
(28) Durgam, G.; Virag, T.; Walker, M.; Tsukahara, R.; Yasuda, S.; Liliom, K.; van Meeteren, L.; Moolenaar, W.; Wilke, N.; Siess, W.; Tigyi, G.; Miller, D. Synthesis, structure−activity relationships, and biological evaluation of fatty alcohol phosphates as lysophosphatidic acid receptor ligands, activators of PPAR gamma, and inhibitors of autotaxin. *J. Med. Chem.* **2005**, *48*, 4919–4930.
(29) Ferry, G.; Moulharat, N.; Pradere, J.-P.; Desos, P.; Try, A.; Genton, A.; Giganti, A.; Beucher-Gaudin, M.; Lonchampt, M.; Bertrand, M.; Saulnier-Blache, J.-S.; Tucker, G. C.; Cordi, A.; Boutin, J. A. S32826: A nanomolar inhibitor of autotaxin: discovery, synthesis and applications as a pharmacological tool. *J. Pharmacol. Exp. Ther.* **2008**, *327*, 809–819.
(30) Gududuru, V.; Zeng, K.; Tsukahara, R.; Makarova, N.; Fujiwara, Y.; Pigg, K. R.; Baker, D. L.; Tigyi, G.; Miller, D. D. Identification of Darmstoff analogs as selective agonists and antagonists of lysophosphatidic acid receptors. *Bioorg. Med. Chem. Lett.* **2006**, *16*, 451–456.
(31) Baker, D. L.; Fujiwara, Y.; Pigg, K. R.; Tsukahara, R.; Kobayashi, S.; Murofushi, H.; Uchiyama, A.; Murakami-Murofushi, K.; Koh, E.; Bandle, R. W.; Byun, H.-S.; Bittman, R.; Fan, D.; Murph, M.; Mills, G. B.; Tigyi, G. Carba analogs of cyclic phosphatidic acid are selective inhibitors of autotaxin and cancer cell invasion and metastasis. *J. Biol. Chem.* **2006**, *281*, 22786–22793.
(32) Jiang, G.; Xu, Y.; Fujiwara, Y.; Tsukahara, T.; Tsukahara, R.; Gajewiak, J.; Tigyi, G.; Prestwich, G. D. Alpha-Substituted phosphonate analogues of lysophosphatidic acid (LPA) selectively inhibit production and action of LPA. *ChemMedChem* **2007**, *2*, 679–690.
(33) van Meeteren, L. A.; Brinkmann, V.; Saulnier-Blache, J.-S.; Lynch, K. R.; Moolenaar, W. H. Anticancer activity of FTY720: phosphorylated FTY720 inhibits autotaxin, a metastasis-enhancing and angiogenic lysophospholipase D. *Cancer Lett.* **2008**, *266*, 203–208.
(34) Parrill, A. L.; Baker, D. L. Autotaxin Inhibition: Challenges and Progress Toward Novel Anti-Cancer Agents. *Anticancer Agents Med. Chem.* **2008**, *8*, 917–923.
(35) Cui, P.; McCalmont, W. F.; Tomsig, J. L.; Lynch, K. R.; Macdonald, T. L. Alpha- and beta-substituted phosphonate analogs of LPA as autotaxin inhibitors. *Bioorg. Med. Chem.* **2008**, *16*, 2212–2225.
(36) Saunders, L. P.; Ouellette, A.; Bandle, R.; Chang, W. C.; Zhou, H.; Misra, R. N.; Cruz, E. M. D. L.; Braddock, D. T. Identification of small-molecule inhibitors of autotaxin that inhibit melanoma cell migration and invasion. *Mol. Cancer Ther.* **2008**, *7*, 3352–3362.
(37) Parrill, A. L.; Echols, U.; Nguyen, T.; Pham, T.-C. T.; Hoeglund, A.; Baker, D. L. Virtual screening approaches for the identification of non-lipid autotaxin inhibitors. *Bioorg. Med. Chem.* **2008**, *16*, 1784–1795.
(38) Moulharat, N.; Fould, B.; Giganti, A.; Boutin, J. A.; Ferry, G. Molecular pharmacology of adipocyte-secreted autotaxin. *Chem.−Biol. Interact* **2008**, *172*, 115–124.
(39) *MOE. 2008.06*; Chemical Computing Group: Montreal, **2003**.
(40) Zalatan, J. G.; Fenn, T. D.; Brunger, A. T.; Herschlag, D. Structural and Functional Comparisons of Nucleotide Pyrophosphatase/Phosphodiesterase and Alkaline Phosphatase: Implications for Mechanism and Evolution. *Biochemistry* **2006**, *45*, 9788–9803.
(41) Ihlenfeldt, W. D.; Voigt, J. H.; Bienfait, B.; Oellien, F.; Nicklaus, M. C. Enhanced CACTVS browser of the Open NCI Database. *J. Chem. Inf. Comput. Sci.* **2002**, *42*, 46–57.
(42) Duan, R. D.; Bergman, T.; Xu, N.; Wu, J.; Cheng, Y.; Duan, J.; Nelander, S.; Palmberg, C.; Nilsson, A. Identification of human

intestinal alkaline sphingomyelinase as a novel ecto-enzyme related to the nucleotide phosphodiesterase family. *J. Biol. Chem.* **2003**, *278*, 38528–38536.
(43) Sakagami, H.; Aoki, J.; Natori, Y.; Nishikawa, K.; Kakehi, Y.; Natori, Y.; Arai, H. Biochemical and molecular characterization of a novel choline-specific glycerophosphodiester phosphodiesterase belonging to the nucleotide pyrophosphatase/phosphodiesterase family. *J. Biol. Chem.* **2005**, *280*, 23084–23093.
(44) Langer, T.; Wolber, G. Pharmacophore definition and 3D searches. *Drug Discovery Today: Technol.* **2004**, *1*, 203–207.
(45) Yang, H.; Shen, Y.; Chen, J.; Jiang, Q.; Leng, Y.; Shen, J. Structure-based virtual screening for identification of novel 11B-HSD1 inhibitors. *Eur. J. Med. Chem.* **2009**, *44*, 1167–1171.
(46) Ueda, S.; Kato, M.; Inuki, S.; Ohno, H.; Evans, B.; Wang, Z.-x.; Peiper, S. C.; Izumi, K.; Kodama, E.; Matsuoka, M.; Nagasawa, H.; Oishi, S.; Fujii, N. Identification of novel non-peptide CXCR4 antagonists by ligand-based design approach. *Bioorg. Med. Chem. Lett.* **2008**, *18*, 4124–4129.
(47) Patani, G. A.; LaVoie, E. J. Bioisosterism: a rational approach in drug design. *Chem. Rev.* **1996**, *96*, 3147–3176.
(48) Rye, C. S.; Baell, J. B. Phosphate Isosteres in Medicinal Chemistry. *Curr. Med. Chem.* **2005**, *12*, 3127–3141.
(49) Zhang, Z.-Y. Protein Tyrosine Phosphatases: Structure and Function, Substrate Specificity, and Inhibitor Development. *Annu. Rev. Pharmacol. Toxicol.* **2002**, *42*, 209–234.
(50) Kotoris, C. C.; Chen, M.-J.; Taylor, S. D. Novel Phosphate Mimetics for the Design of Non-peptidyl Inhibitors of Protein Tyrosine Phosphatases. *Bioorg. Med. Chem. Lett.* **1998**, *8*, 3275–3280.
(51) Stefan, C.; Jansen, S.; Bollen, M. NPP-type ectophosphodiesterases: unity in diversity. *Trends Biochem. Sci.* **2005**, *30*, 542–550.
(52) Gijsbers, R.; Aoki, J.; Arai, H.; Bollen, M. The hydrolysis of lysophospholipids and nucleotides by autotaxin (NPP2) involves a single catalytic site. *FEBS Lett.* **2003**, *538*, 60–64.
(53) Clair, T.; Koh, E.; Ptaszynska, M.; Bandle, R.; Liotta, L.; Schiffmann, E.; Stracke, M. L-Histidine inhibits production of lysophosphatidic acid by the tumor-associated cytokine, autotaxin. *Lipids Health Dis.* **2005**, 4.
(54) North, E. J.; Osborne, D. A.; Bridson, P. K.; Baker, D. L.; Parrill, A. L. Autotaxin structure−activity relationships revealed through lysophosphatidylcholine analogs. *Bioorg. Med. Chem.* **2009**, *17*, 3433–3442.
(55) Halgren, T. A. Merck Molecular Force Field. I. Basis, Form, Scope, Parameterization, and Performance of MMFF94*. *J. Comput. Chem.* **1996**, *17*, 490–519.